Electronic Supplementary Material (ESI) for Inorganic Chemistry Frontiers.

Supporting information

Bifunctional Electroreduction Catalysts of NiFe Alloy on N-doped Carbon toward Industrial-level CO_2 Conversion Powered by Zn-air Batteries

Songjiang Wu,[a+] Haiyan Chen,[a+] Chunguang Jia,[a] Li Liao,[a] Kai Chen,[b] Suqin Ci,[a*] Qiuhua Xu,[a] Zhenhai Wen[a,b*]

a Key Laboratory of Jiangxi Province for Persistent Pollutants Control, National-Local Joint Engineering Research Center of Heavy Metals Pollutants Control and Resource Utilization and Resources Recycle, Nanchang Hangkong University, Nanchang 330063, Jiangxi, China

b CAS Key Laboratory of Design and Assembly of Functional Nanostructures, and Fujian Provincial Key Laboratory of Materials and Techniques toward Hydrogen Energy, Fujian Institute of Research on the Structure of Matter, Chinese Academy of Sciences, Fuzhou, Fujian, 350002, China

** Corresponding authors*

+ These authors contributed equally to this work

E-mail: sqci@nchu.edu.cn, wen@fjirsm.ac.cn

Experimental

Preparation of catalyst

Materials

All regents and chemicals were acquired commercially and utilized without any additional purification. The sources of these chemicals were as follows: $Ni(OAc)_2 \cdot 4H_2O$ was procured from Sigma-Aldrich, $Zn(NO_3)_2 \cdot 6H_2O$ from Macklin, $Fe(NO_3)_3 \cdot 9H_2O$, KOH (90 wt%) and ethanol from Sinopharm, 2-methylimidazole (2-MeIM) from Macklin, Nafion solution (5 wt%) from DuPont, and Pt/C (20%, Macklin).

Preparation of NiFe-ZIF-8

To prepare the catalyst, 2.3 g quantity of 2-methylimidazole (2-MeIM) was dissolved in 50 mL of methanol by sonication for 5 min. Separately, a mixture containing 1.04 g of $Zn(NO_3)_2 \cdot 6H_2O$, 60 mg of $Ni(OAc)_2 \cdot 4H_2O$, and 60 mg of $Fe(NO_3)_3 \cdot 9H_2O$ in 50 mL of methanol was sonicated until a transparent solution was obtained. The resulting solution was then added to the 2-MeIM solution and stirred for 24 h at 60 ℃. The precipitate was collected via centrifugation, washed several times with methanol, and dried under vacuum at 60 ℃ overnight.

Preparation of NiFe-NC

NiFe-NC was successfully synthesized utilizing a facile pyrolysis approach. Initially, NiFe-ZIF-8 powder was subjected to heating in an Ar atmosphere at a rate of 5 ℃/min until it reached a temperature of 1000 ℃, after which it was maintained at this temperature for 3 h. The resulting product was then allowed to naturally cool to room temperature. Moreover, the synthesis of NiFe-NC-900 and NiFe-NC-1100 involved altering the pyrolysis temperature to 900 ℃ and 1000 ℃, respectively. In order to synthesize Ni-NC, Fe-NC, and NC, the same procedure as above was utilized, with the exclusion of $Fe(NO_3)_3 \cdot 9H_2O$ and $Ni(OAc)_2 \cdot 4H_2O$, respectively.

Characterization

We conducted X-ray diffraction (XRD) measurements on a D8 Advance X-ray diffractometer (Bruker, Germany) using Cu-Kα radiation (λ= 0.15406 nm). Raman

spectra were obtained using a LabRAM HR spectrometer. X-ray photoelectron spectroscopy (XPS) was performed on an ESCALAB 250Xi (Thermo Scientific) XPS spectrometer with Al Kα excitation source (1486.6 eV). Scanning electron microscope (SEM) and transmission electron microscope (TEM) images were taken using SU-8010 and Talos F200X (FEI, USA), respectively.

Electrochemical measurements

The electrochemical measurements were conducted in a standard three-electrode configuration using a CHI 660E electrochemical workstation. The potentials were referenced to the reversible hydrogen electrode (RHE) and converted utilizing the following formula: $E_{\mathrm{RHE}} = E_{\mathrm{Hg/HgO}} + 0.098 + 0.059 \times \mathrm{pH}$ (alkaline medium) or $E_{\mathrm{RHE}} = E_{\mathrm{Ag/AgCl}} + 0.197 + 0.059 \times \mathrm{pH}$ (neutral medium). All the electrochemical data were measured without internal resistance (iR) compensation.

CO_2RR measurement

To prepare the catalyst ink, 5 mg of the catalyst was dispersed in a solution containing Nafion (50 μL), ethanol (350 μL), and water (100 μL) using ultrasonic dispersion for 30 min.

The Faraday efficiency of the gas products was calculated using the following equation:

$$\mathrm{FE} = \frac{e_{output}}{e_{input}} \times 100\% = \frac{N_{(CO/H_2)} \times n \times F}{I \times t} \quad (1)$$

$$t = \frac{60 \times v}{r}\ \text{Second} \quad (2)$$

where FE is the Faraday efficiency of a particular product, e_{input} and e_{output} represent the total charge provided and the charge used for the reduction of the product, respectively. $N_{(CO/H2)}$ is the number of moles of CO or H_2 product (measured by GC), n is the number of electrons transferred to produce 1 mole of the product, with a value of 2 for CO and H_2. F is the Faraday constant (96485 C mol^{-1}), I is the test current density, t is the time taken for the sample to fill the loop, v is the volume of the loop, and r is the CO_2 flow rate.

CO_2RR measurement in H-cell

All electrochemical measurements were performed in a custom-built H-cell system, which was equipped with a Nafion 117 membrane to separate the anode and cathode compartments. The counter electrode was a Pt mesh (1 × 1 cm^2), and the reference electrode was an Ag/AgCl electrode (saturated KCl). The working electrode was prepared by depositing a carbon paper (CP, 1 × 1 cm^2) with the catalyst ink (1 mg cm^2). The electrochemical reduction of CO_2 was conducted in an electrolyte of 0.5 M $KHCO_3$, which was thoroughly saturated with CO_2 for over 30 min before each test, with a constant CO_2 flow rate of 20 cm^3 min^{-1}. During the experiments, the cathode chamber was connected to an online gas chromatograph (GC9860), equipped with a PQ column and a TCD detector to continuously analyze the gas products.

CO_2RR measurement in flow cell

The flow cell electrolyzer testing was conducted using a home-made flow cell. A gas diffusion electrode was fabricated by carefully drop-coating 1 mg cm^{-2} of catalyst onto a 1 × 1 cm^2 CP electrode. To ensure complete evaporation, the electrode was placed under an infrared lamp. A Ni foam was used as the OER catalyst in the anodic chamber. A cation exchange membrane (Nafion 117) was sandwiched between the cathode and anode compartments. The cathode compartment was continuously supplied with 3 M KCl, while the anode compartment was supplied with 1 M KOH, both of which were circulated using a pump. Throughout the test, a continuous flow of 20 cm^3 min^{-1} CO_2 was delivered to the cathode, the gas products detected by GC.

ORR measurement

The working electrode was prepared by dispersing 5 mg of the as-synthesized catalyst in a mixture of 400 μL water, 50 μL of Nafion, and 50 μL of ethanol under ultrasonic treatment. 6 μL of the resulting homogeneous ink was coated onto the glass carbon electrode (GCE)/rotating disc electrode (RDE). The electrochemical measurements were conducted in 1.0 M potassium hydroxide (KOH) electrolyte using a three-electrode system with a CHI 760E Electrochemical Workstation (CH Instruments, Shanghai, Chenhua Co., Ltd.) The catalyst-coated GCE/RDE was utilized

as the working electrode, while Hg/HgO electrode, and Pt wire were employed as the reference electrode and counter electrode, respectively. The ORR test was conducted using Linear sweep voltammetry (LSV) with a scan rate of 5 mV s^{-1} in O_2-saturated 0.1 M KOH electrolyte.

The electron transfer number (n) was acquired by the Koutecky- Levich (K-L) Eq:

$$\frac{1}{J} = \frac{1}{J_L} + \frac{1}{J_K} = \frac{1}{B\omega^{1/2}} + \frac{1}{J_K} \quad (3)$$

$$B = 0.2nFC_0D_0^{2/3}v^{-1/6} \quad (4)$$

$$J_K = \frac{1}{nkFC_0} \quad (5)$$

The variables in the study are denoted as follows: J, J_K and J_L represent the tested current density, kinetic current density, and limiting diffusion current density, respectively, measured in mA cm^{-2}. The variable ω indicates the rotation speed of the rotating disk electrode, expressed in rpm min^{-1}. F represents the Faraday constant, which has a value of 96485 C mol^{-1}. C_0 and D_0 refer to the volume concentration and diffusion coefficient of O_2, respectively. In a 0.1 mol L^{-1} KOH solution, C_0 is equal to 1.2×10^{-3} mol cm^{-3}, while D_0 is 1.9×10^{-5} cm^2 s^{-1}. The kinematic viscosity of the electrolyte is represented by the variable ν, which has a value of 0.01 cm^2 s^{-1} in a 0.1 mol L^{-1} KOH solution. Finally, k is the electron transfer rate constant.

Zn-air batteries (ZAB) measurements

A uniformly dispersed catalyst slurry was prepared by mixing 5 mg of cathode catalyst with 400 μL of water, 50 μL of ethanol, and 50 μL of Nafion solution, followed by sonication for 30 min. 100 μL of the resulting catalyst slurry was drawn up using a pipette and coated onto a 1 cm^2 carbon paper substrate. After drying, the cathode was used for testing, with a loading amount of 1 mg cm^{-2}. The anode consisted of pure zinc with a surface area of 1 cm^2, and the electrolyte solution used was a mixture of 6 mol L^{-1} KOH and 0.2 mol L^{-1} zinc acetate. LAND testing system was used to measure the data of ZAB.

Assembly and tests of ZABs-powered CO_2 flow electrolysis system

Two ZABs are connected in series with a flow electrolytic cell (without reference electrode) and a 10 Ω resistor. The voltage across the resistor is collected using a voltage collector with a frequency of 200 s, and then the current density of the system at that time is calculated using the formula:

$$I = \frac{U}{R} \tag{6}$$

DFT calculations

DFT parameters

All the calculations are implemented by PWSCF codes contained in the Quantum ESPRESSO distribution[1]. Spin-polarized DFT calculations were performed with periodic super-cells under the generalized gradient approximation (GGA) using the Perdew-Burke-Ernzerhof (PBE) functional for exchange-correlation and the ultrasoft pseudopotentials for nuclei and core electrons. The Kohn-Sham orbitals were expanded in a plane-wave basis set with a kinetic energy cutoff of 30 Ry and the charge-density cutoff of 300 Ry. The Fermi-surface effects has been treated by the smearing technique of Methfessel and Paxton, using a smearing parameter of 0.02 Ry. Periodical supercells containing single-layer graphene with 15 Å vacuum above were used to model various graphene doping structures. To model the doping N in the basal plane, we used the super cell of lateral size 4 × 4. For the doping N in the edge, we used the super cell of lateral size 3 × 5. We added 8 atoms of metal clusters, half each of NiFe alloy, underneath these active sites of graphitic carbon to simulate the graphene-covered metal cluster structure. For Ni (111), Fe (111) and NiFe (111) a 1×1 supercell and eight-layer slab is utilized. The bottom four-layer is fixed to model Ni, Fe and NiFe bulk. The Brillouin zone was sampled with (1 × 1 × 1) Monkhorst–Pack k-points.

Virtual energetic span as the activity determining term

Norskov's approach uses the largest Gibbs energy (ΔGmax) as the activity determining term. This descriptor is proposed under the assumption of so-called "rate determining step assumption": the slowest step should control the total kinetic of a series process[2]. Wever, for a multi-step reaction that takes place at limited position, such

as catalytic reaction, it has been gradually noticed in last ten years that there is no such thing of a "rate determining step" (RDS), instead, there should be a "rate determining state"[3]. That is, the catalytic activity should be co-determined by several steps. Based on such idea, one should avoid use ΔG^{max}, but to build some newly proposed descriptor that abandon the using of RDS. There are now two such kinds of descriptors, one is the highest free energy of an reaction intermediate (denoted as G_{max} (RI)) proposed by Exner *et al*[4]. The other is the "virtual energetic span" (δE^{v}) proposed by us[5]. And we will use the latter as the activity determining term in this paper.

The "virtual energetic span" (δE^{v}) comes from the "energetic span" that proposed by Kozuch *et al*[6]. It is the simplification of the result of a full microkinetic model. We won't go into too much details here because it have given detailed illustration in ref [5]. Here we only give its brief conclusion: to use the virtual energetic span, we can still follow the basic principle of Norskov's method, to build a *TS*-free FED. What is different from Norskov's approach is we can treat the mid-point of each joint line in FED, as the "virtual transition states (*TS*v)". We name it virtual transition state because it is not the real energy of the transition state, but it has a constant difference to the real energy of the transition state. This can be strictly proved under the method of Norskov. Among those TS^{v}, there is one that determines the turnover frequency (TOF), we name it the TOF determining TS^{v}, aliased as $TDTS^{v}$. On the other hand, for the energies of the intermediates, that is, the energy levels of the steps in FED, there is also one step that determines the activity. It is named as the TOF determining intermediate (*TDI*). The δE^{v} is calculated simply by the difference between $TDTS^{v}$ and *TDI*:

$$\delta E^{v} = TDTS^{v} - TDI \quad \text{(S1)}$$

When obtaining the δE^{v}, the TOF can be simply calculated by

$$TOF = k_0 \exp\left(-\delta E^{v}/RT\right) \quad \text{(S2)}$$

The result should be the same as that deduced from a complete microkinetic model. So, the only question left would be the definitions of $TDTS^{v}$ and *TDI*. We can collect all the energy of the intermediates[7], and the all the energies of the TS^{v} $\{TS^{v}_{i}\}$. Then we

pick one TS^{v}_{i} and one $\{I_i\}$. The difference between them should form a new set: $\{TS^{v}_{i} - I_j\}$. In this set, we add an element ΔG^{r}_{ij}, which will lead the general term formula of the set to be: $\{TS^{v}_{i} - I_j + \Delta G^{r}_{ij}\}$, where ΔG^{r}_{ij} is expressed as:

$$\Delta G^{r}_{ij} = \begin{cases} n\eta e & if\ \ i < j\ (means\ I_j\ locates\ after\ TS_i^{v}) \\ 0 & if\ i > j\ (means\ I_j\ locates\ before\ TS_i^{v}) \end{cases} \quad \text{(S3)}$$

With n and η the total electron transfer number and the applied overpotential. $TDTS^{v}$ and TDI are then the $TS^{v}_{i} - I_j$ that will maximize $\{TS^{v}_{i} - I_j + \Delta G^{r}_{ij}\}$.

A brief introduction of the computational hydrogen electrode (CHE) method.

Generally speaking, when studying about the electrocatalytic reaction through first principle, there are two difficulties, one is to calculate the reaction barrier of the proton coupled electron transfer (PCET) reaction, the other is the Gibbs free energy of the solvated H^+. The CHE method[8] proposed by Norskov et al is aiming at settling or bypassing these two difficulties. In the framework of CHE method, for the reaction

$$H^+ + e \rightarrow 1/2H_2 \quad \text{(S4)}$$

reaches equilibrium on U_{SHE}=0 V, one can replace the energy of H^+ with that of $1/2H_2$:

$$G_{H+} = 1/2G_{H2} \quad \text{(S5)}$$

The energy of electron can be expressed by –Ue, where U is the electrode potential *vs.* SHE. As for the reaction barrier of PCET, the CHE method assumes the overpotential of the electrocatalytic reaction is the overpotential least to make standard reaction Gibbs free energies of all the elementary step to be exothermic. And such potential is called the reaction limiting potential, which is denoted as U_l. Usually, U_l is an activity descriptor, as for CO_2RR, U_l can be used to judge the exact reaction pathway.

The reaction models and pathway

The reaction mechanisms for CO2RR written as follows:

$$CO_2 + H^+ + e + * \rightarrow COOH* \quad \text{(S6)}$$

$$COOH* + H^+ + e \rightarrow CO* + H_2O(l) \quad \text{(S7)}$$

$$CO* \rightarrow CO(g) + * \quad \text{(S8)}$$

The asterisk stands for the sites on the surface of the catalysts.

In calculating the Gibbs free energy differences from R4 to R8, the associated

adsorption free energy of the adsorbates are calculated by the following expression:

$$G_A = E_A + ZPE - TS + \int C_p dT \quad \text{(S9)}$$

Where E_A is the total energy of a certain molecule or adsorbate A*. When A is representing a certain molecule, the total energies can be calculated directly. When A is representing a certain adsorbate, it is calculated by the difference between the DFT based substrate with (E_{A*}^{DFT}) and without adsorbate A (E_*^{DFT}):

$$E_A = E_{A*}^{DFT} - E_*^{DFT} \quad \text{(S10)}$$

ZPE, TS and $\int C_p dT$ are the correction from zero point energy, entropy and heat capacity, whose values are listed on Table S1. Other than that, H^+ is calculated by the Gibbs free energy of $1/2H_2$, the energy of electron is calculated by $-Ue$. A correction of -0.51 eV is added to CO molecules for the errors for GGA-PBE functional. According to Ref.[9]. such correction can lead an agreement with experimental overall half reaction of CO_2 reduction.

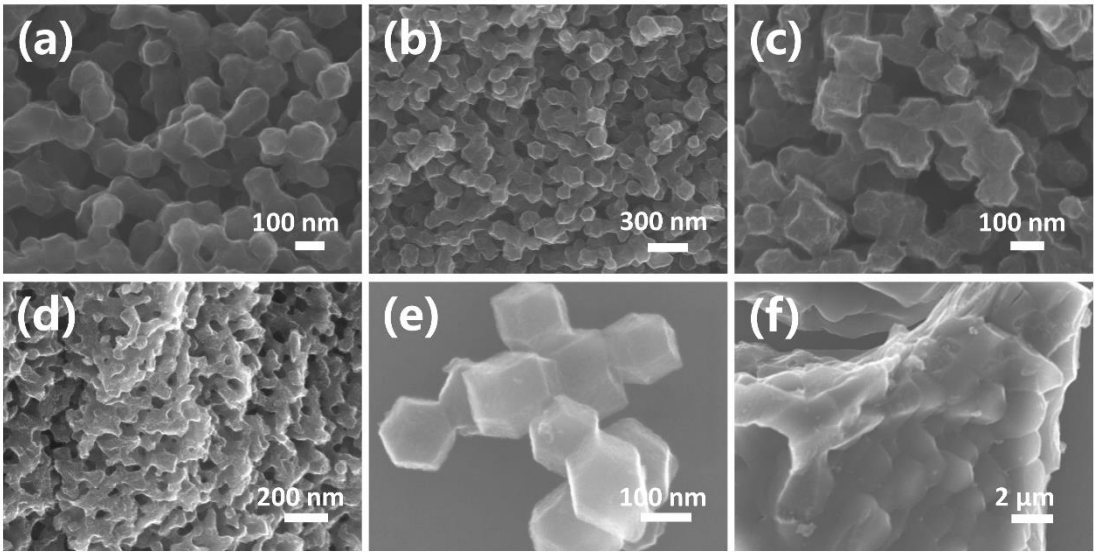

Figure S1 SEM images of (a) NiFe-NC-900, (b) NiFe-NC, (c) NiFe-NC-1100, (d) Ni-NC, (e) Fe-NC, and (f) NC.

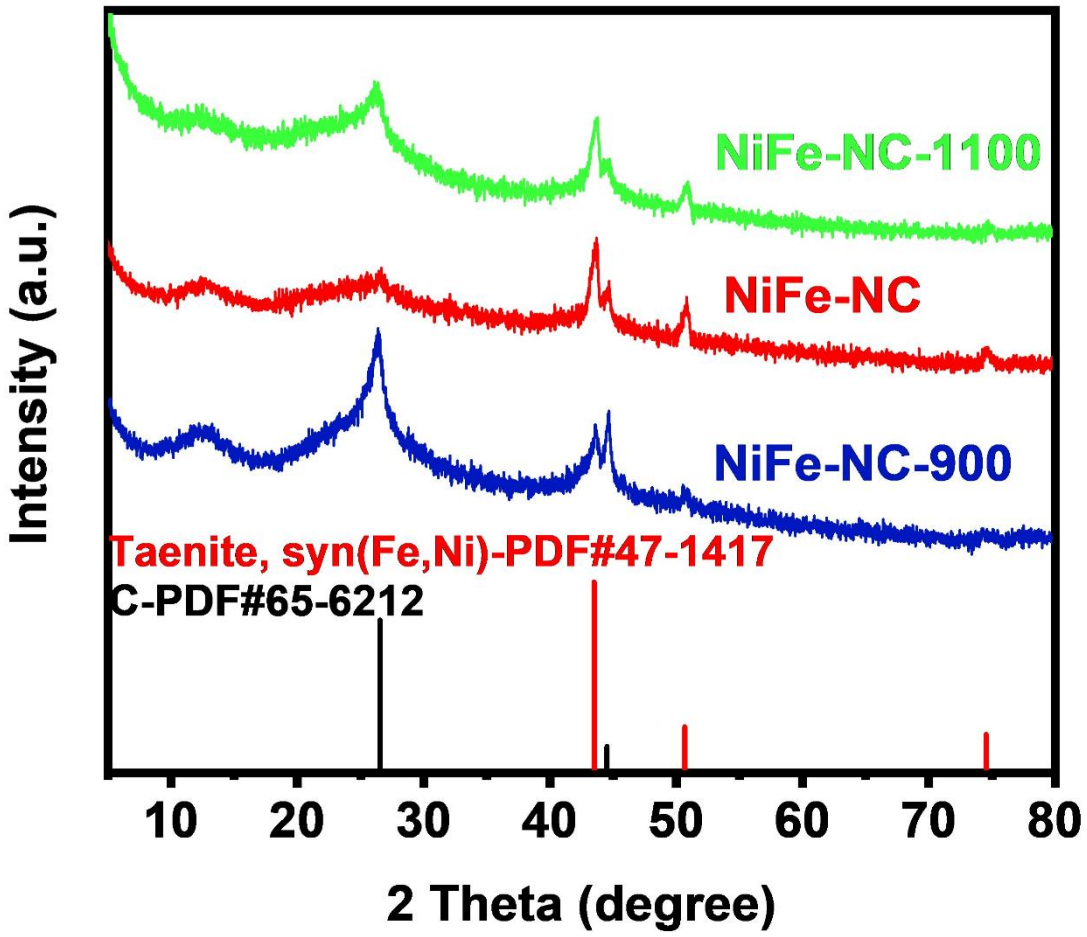

Figure S2 XRD patterns of NiFe-NC-900, NiFe-NC-1000, and NiFe-NC-1100.

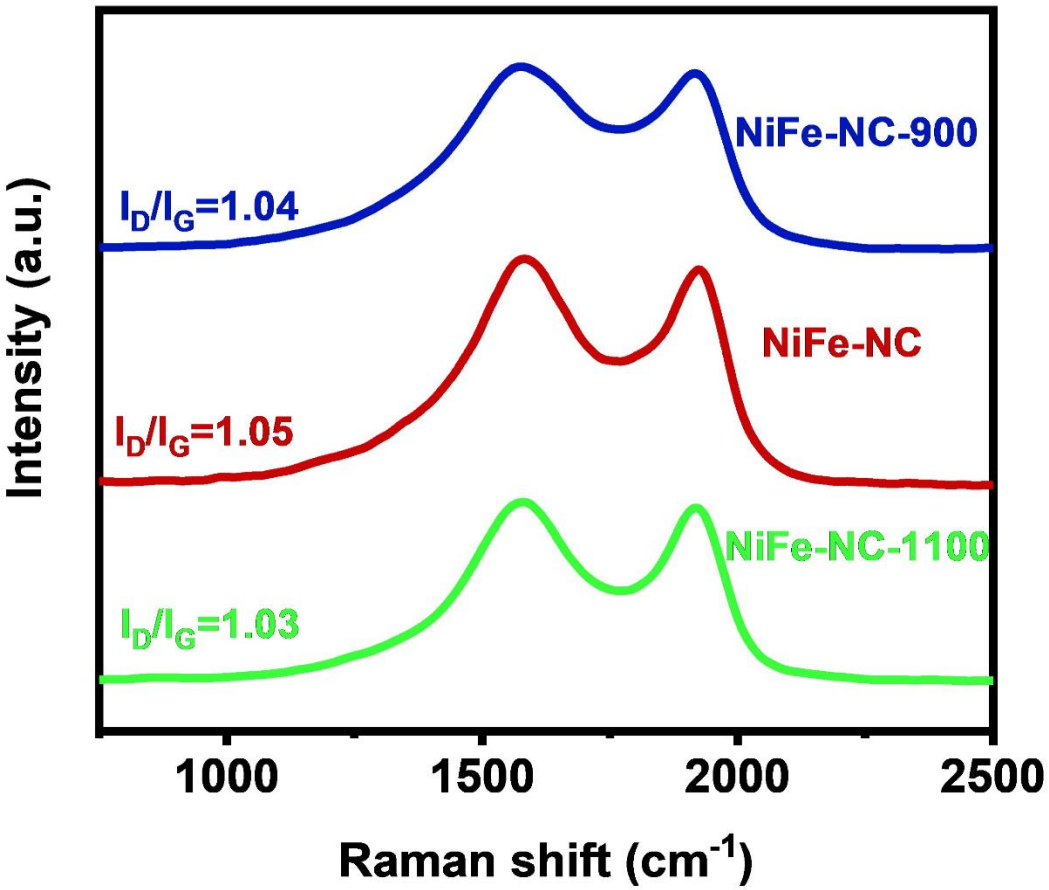

Figure S3 Raman spectra of NiFe-NC-900, NiFe-NC, and NiFe-NC-1100.

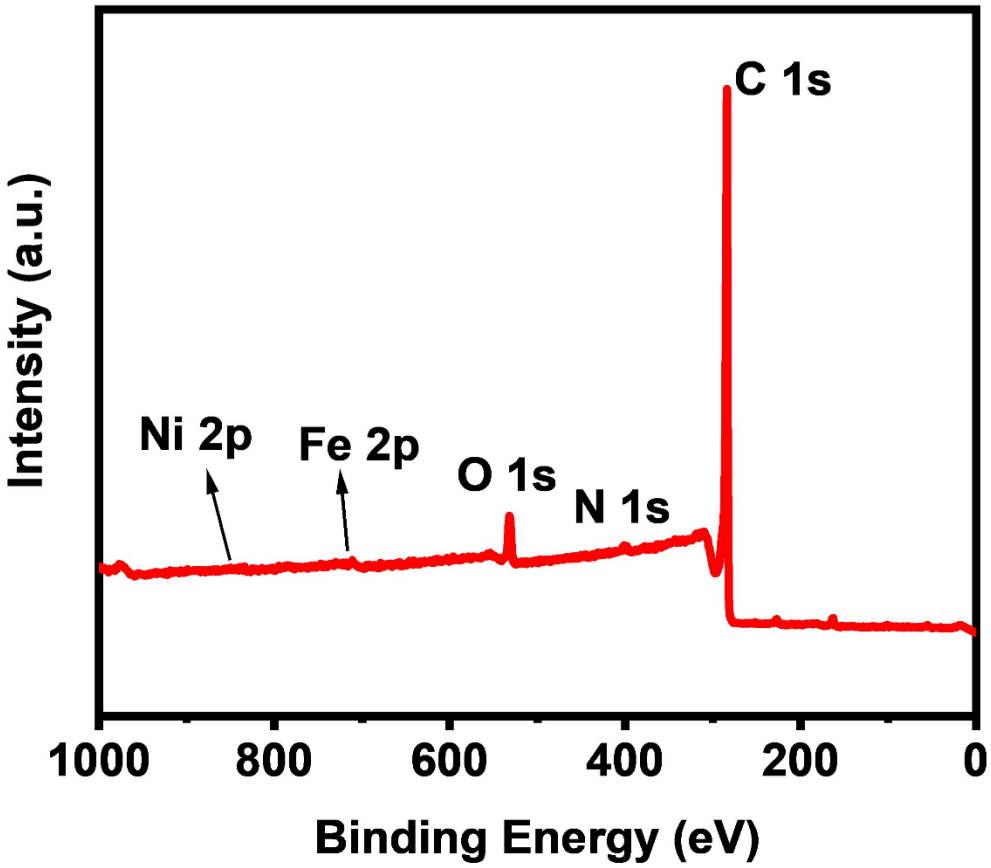

Figure S4 The XPS survey of NiFe-NC.

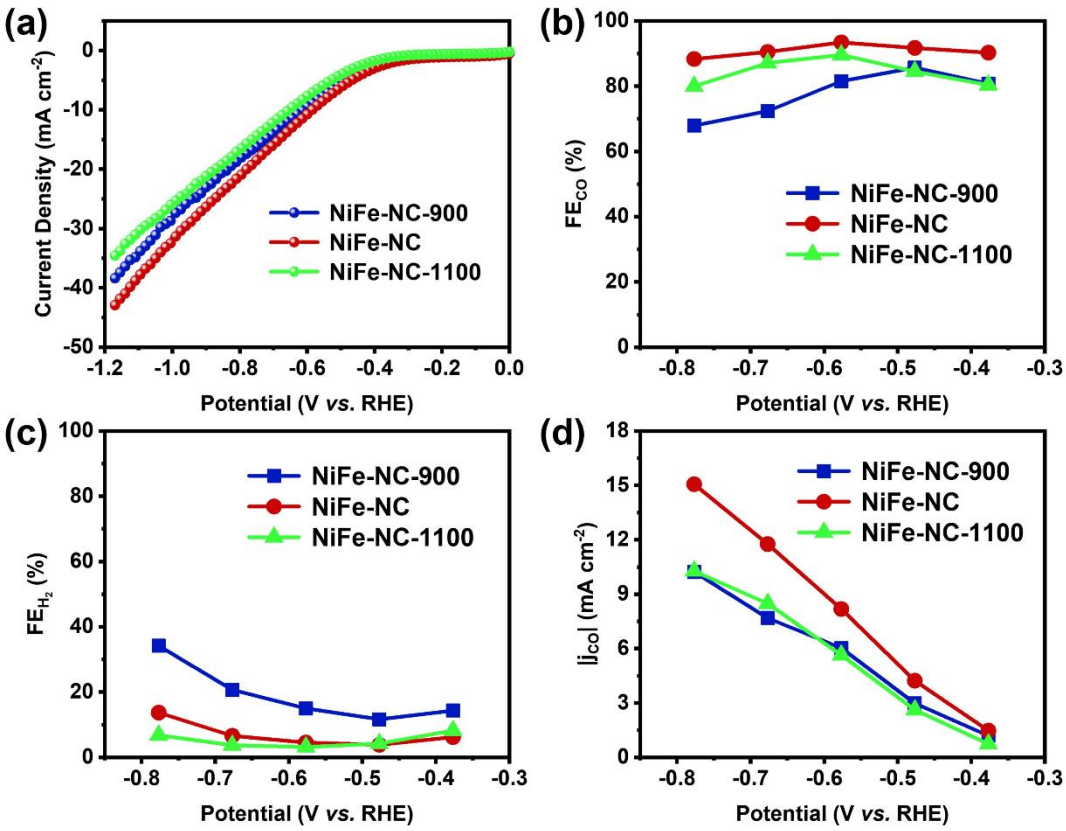

Figure S5 (a) LSV curves of the prepared catalysts measured in CO_2-saturated 0.5 M $KHCO_3$ electrolyte; (b) FE_{CO} and (c) FE_{H2} of the prepared catalysts; (d) CO partial current density of the prepared catalysts.

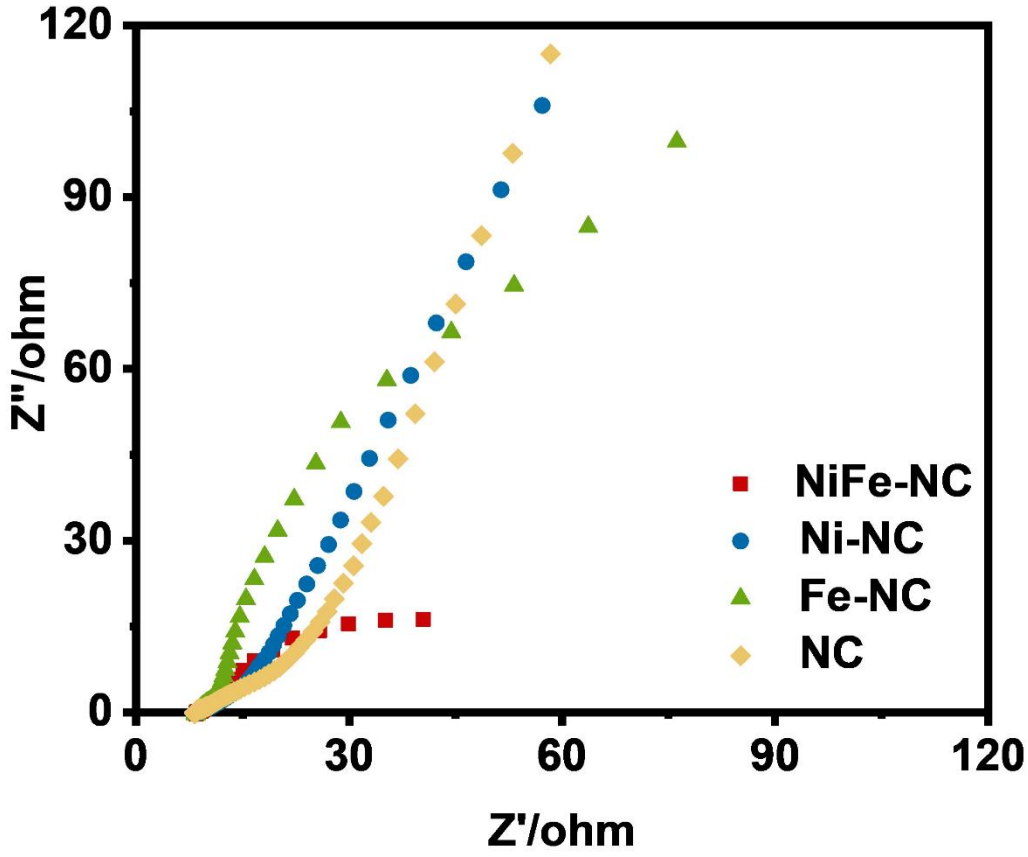

Figure S6 EIS spectrum at -0.3 V *vs.* RHE.

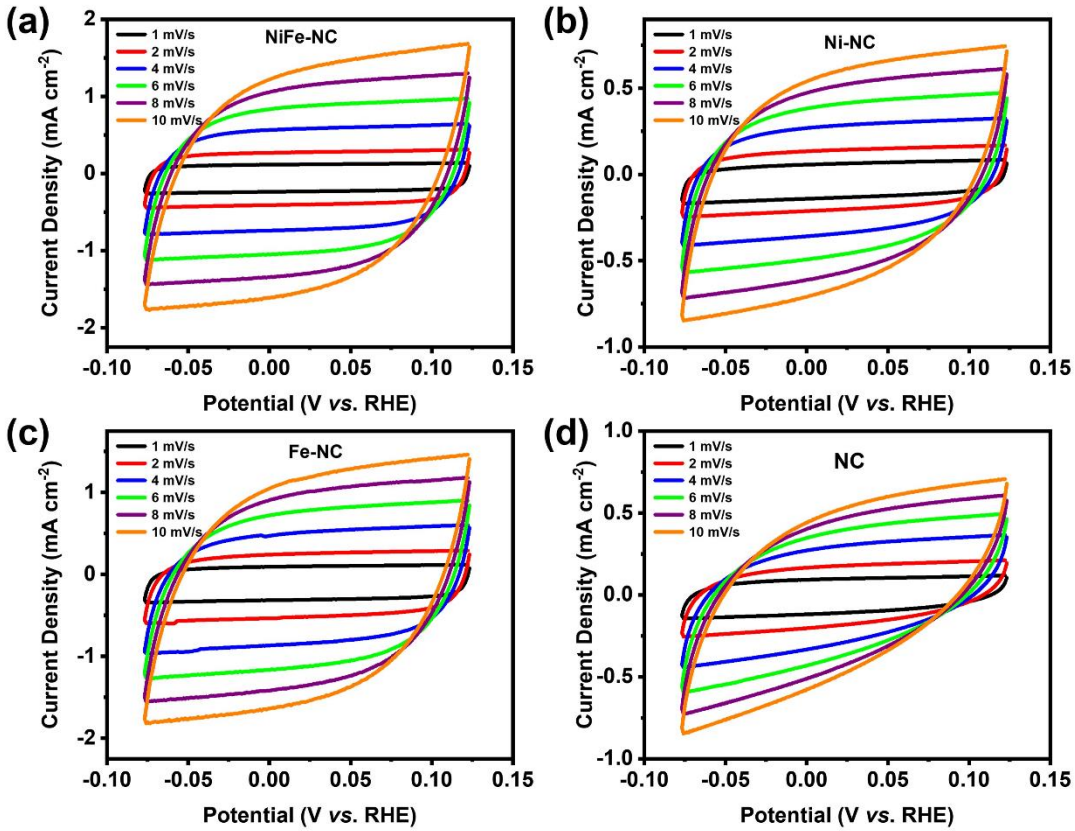

Figure S7 (a-d) CV curves at different scan rates.

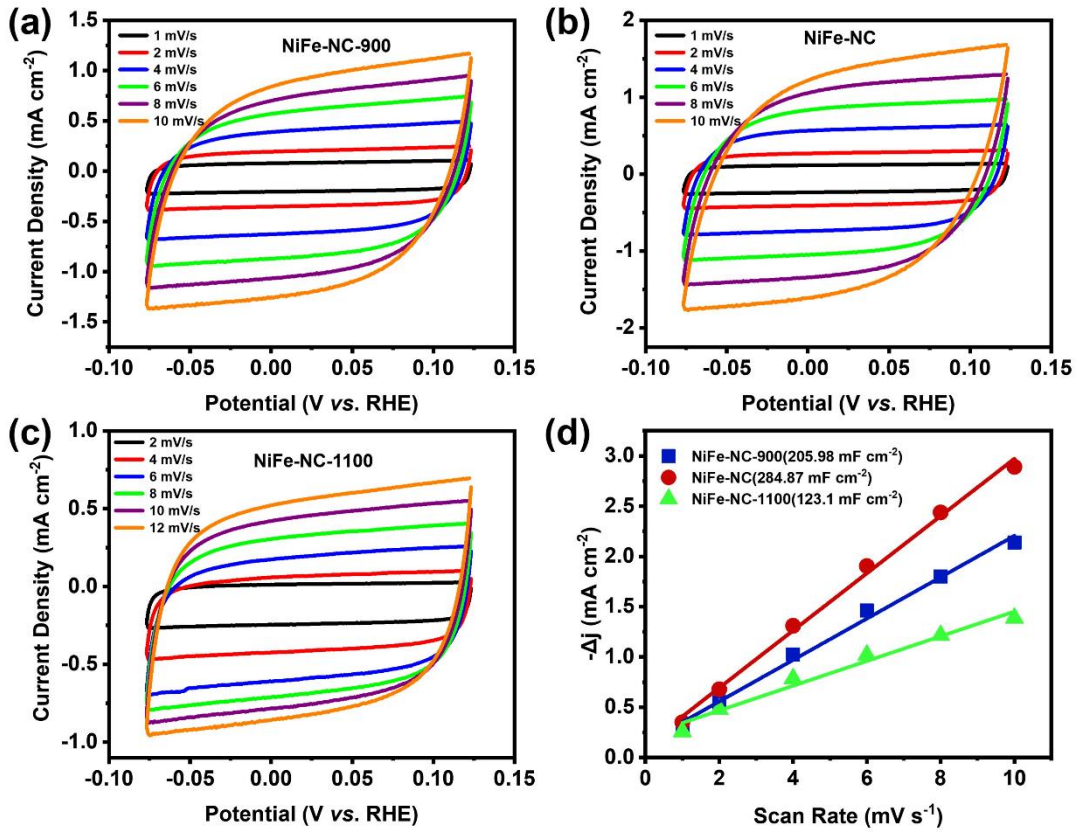

Figure S8 (a-c) CV curves at different scan rates. (d) The double-layer capacitance (Cdl) of different samples.

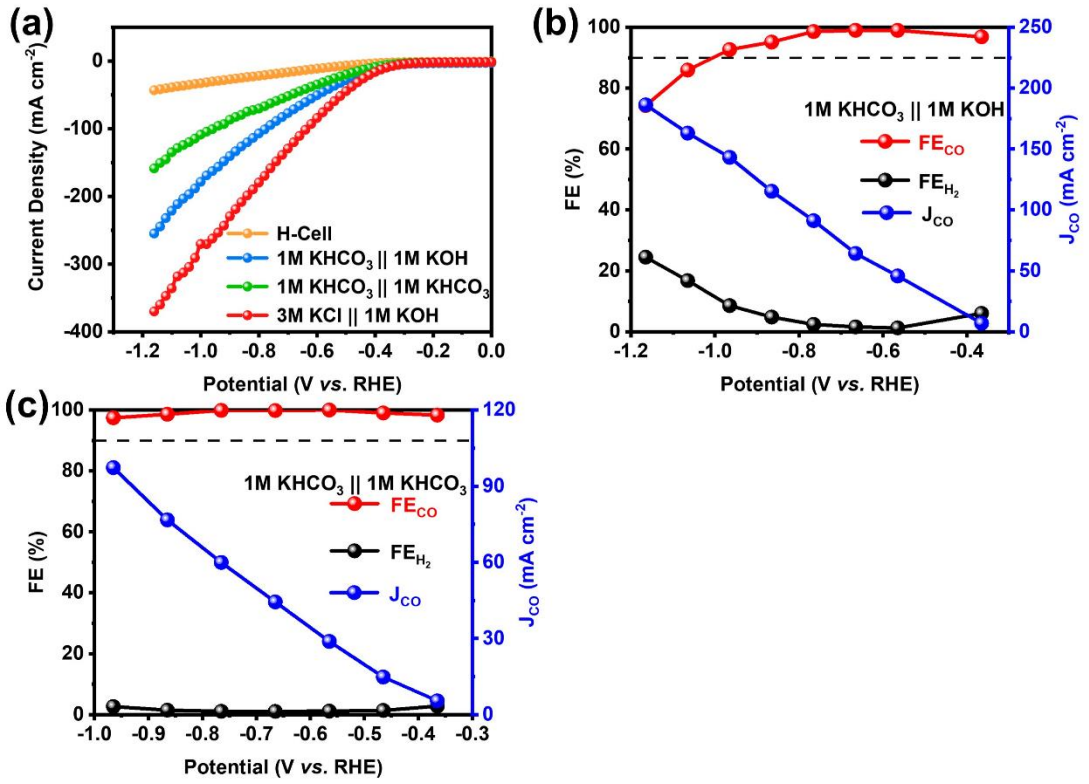

Figure S9 (a) LSV curves of NiFe-NC measured in flow cell (in different electrolytes). (b-c) FE_{CO} and corresponding current densities of NiFe-NC in flow cell (in different electrolytes).

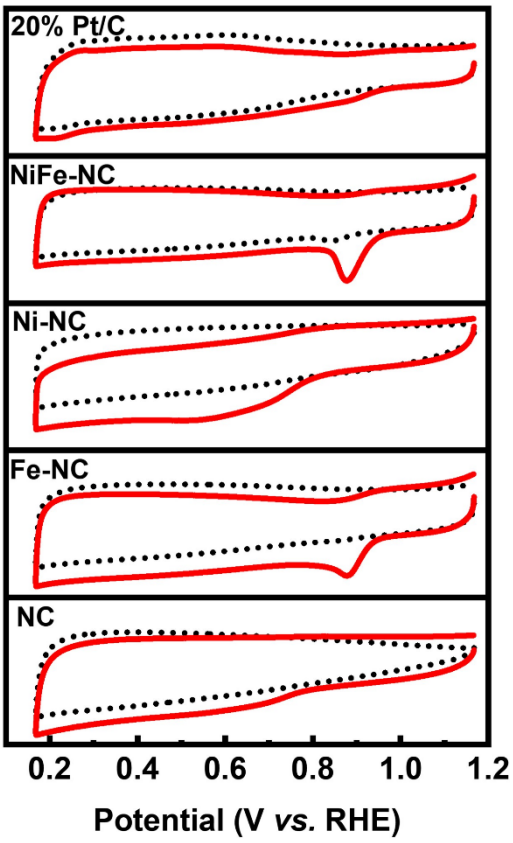

Figure S10 CVs of catalysts in Ar and O_2 saturated 0.1 M KOH, at a scan rate of 50 mV s^{-1}.

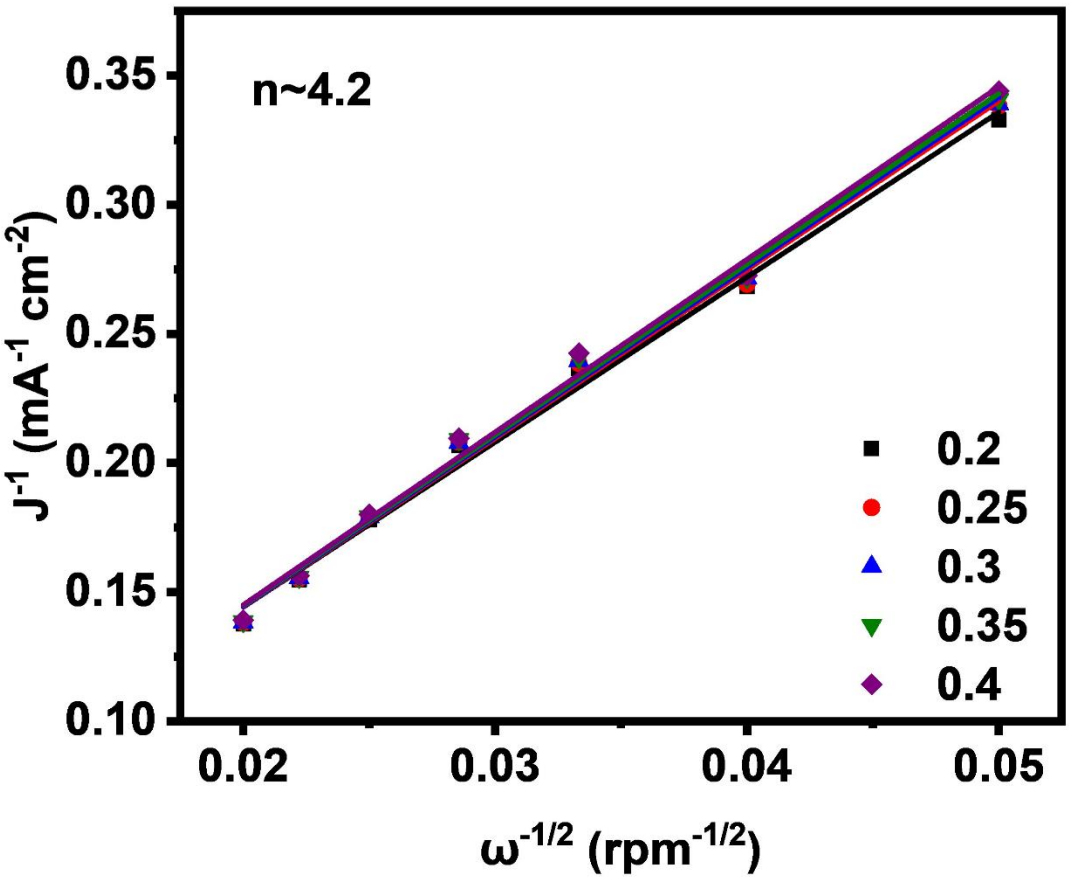

Figure S11 K-L plots for NiFe-NC and the electron transfer number at various potentials.

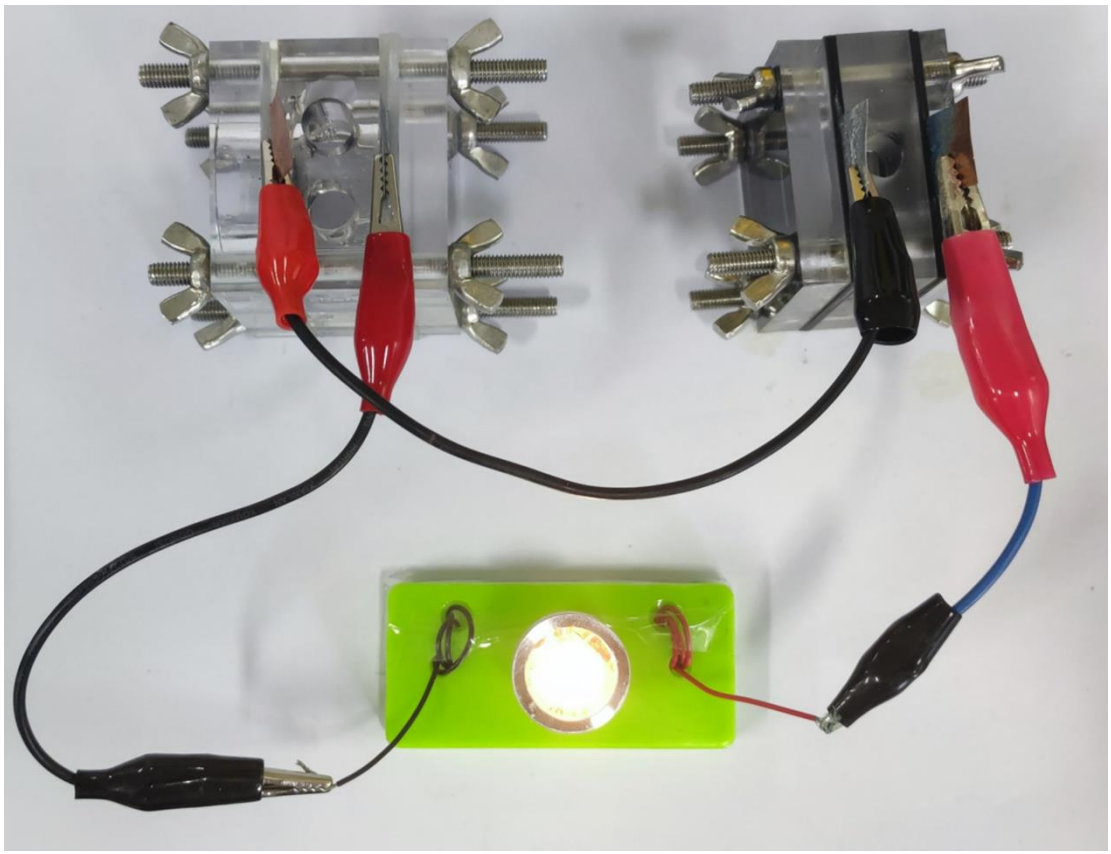

Figure S12 the physical picture of Zn-air battery with NiFe-NC and a small bulb being lighted by ZAB

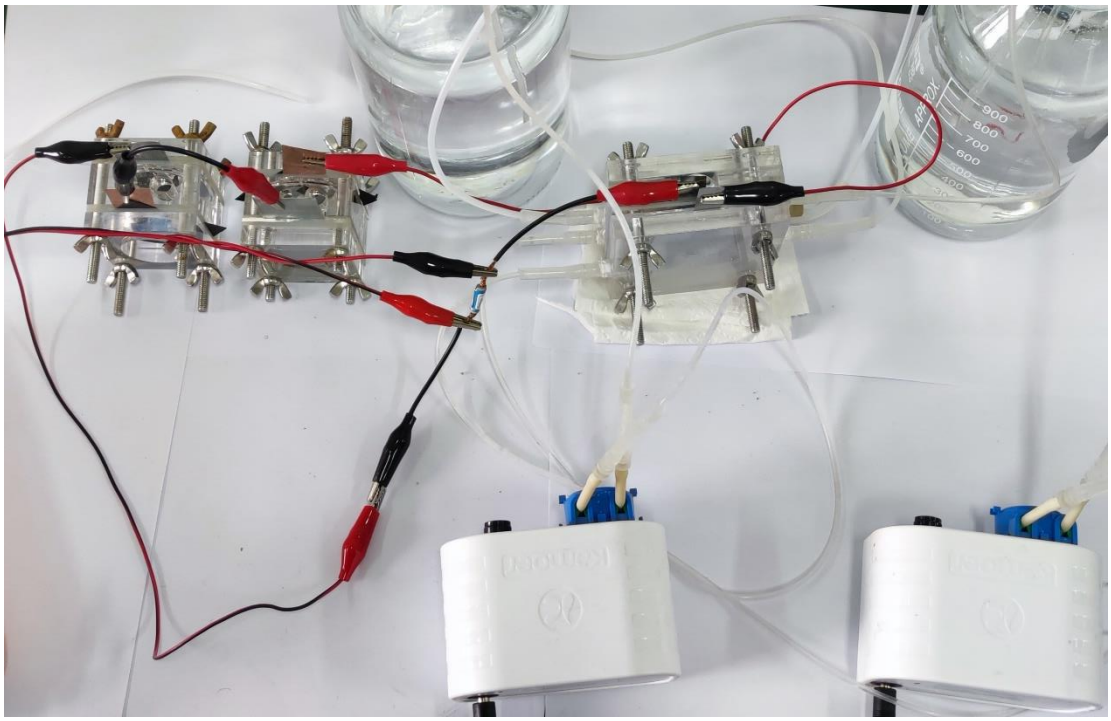

Figure S13 the photograph of self-driven CO_2 flow electrolysis system

Figure S14 the voltage across the resistor

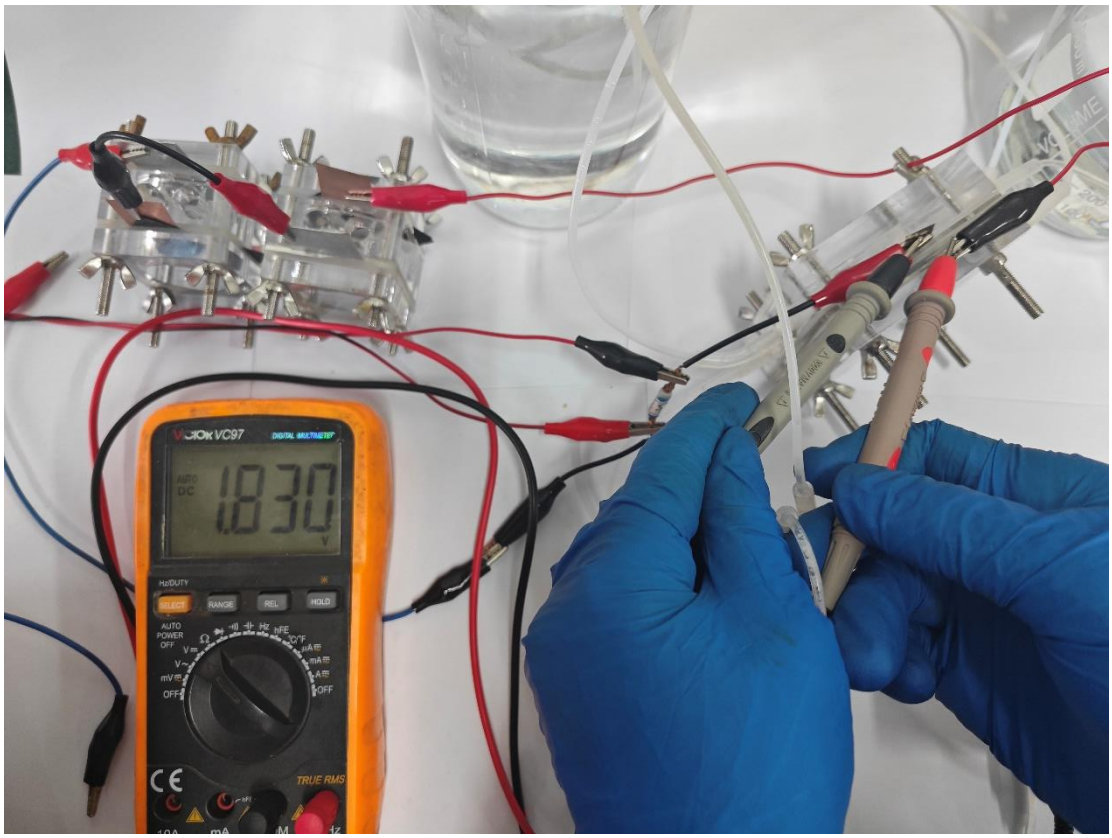

Figure S15 the voltage across the CO_2 flow electrolytic system

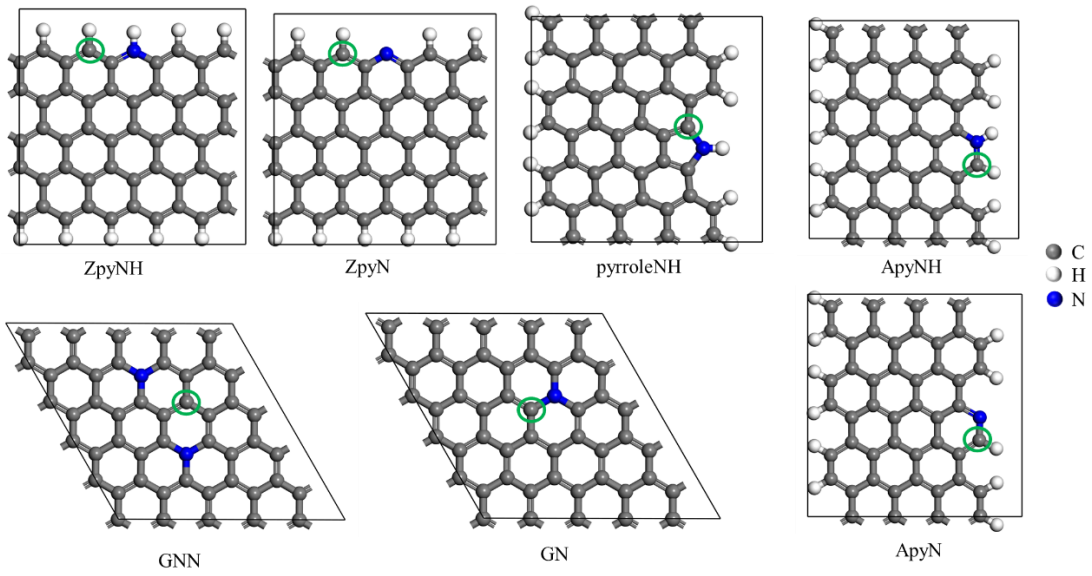

Figure S16 N doped graphene structure, green circle is the active site

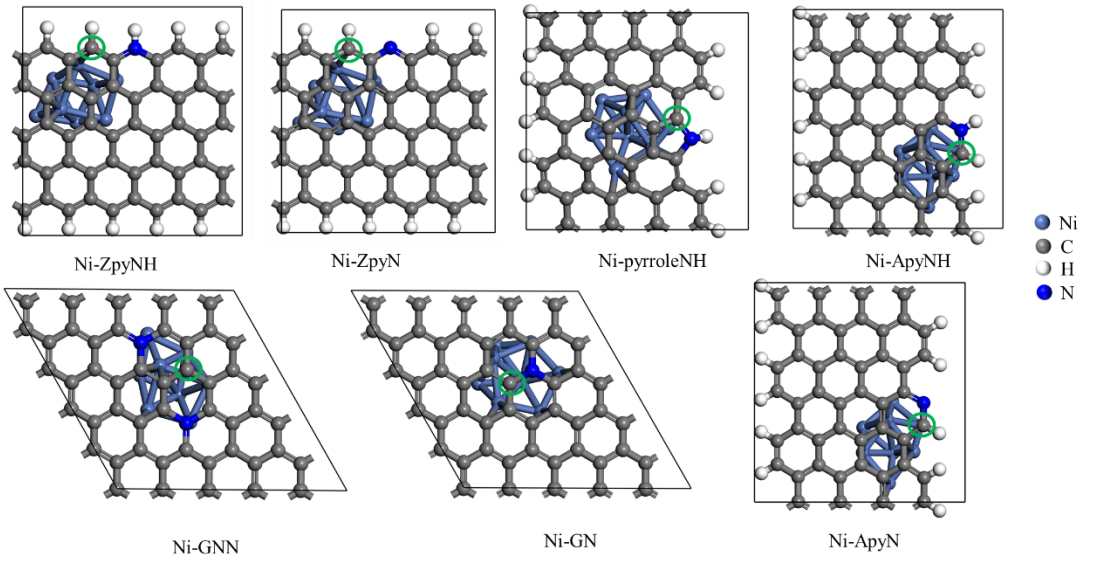

Figure S17 graphene-covered Ni clusters.

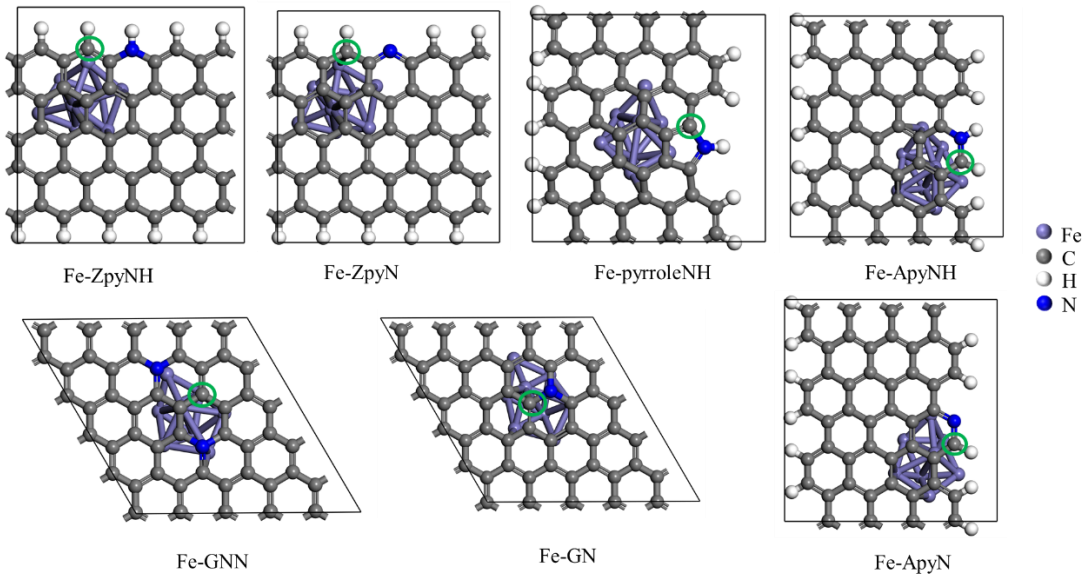

Figure S18 graphene-covered Fe clusters.

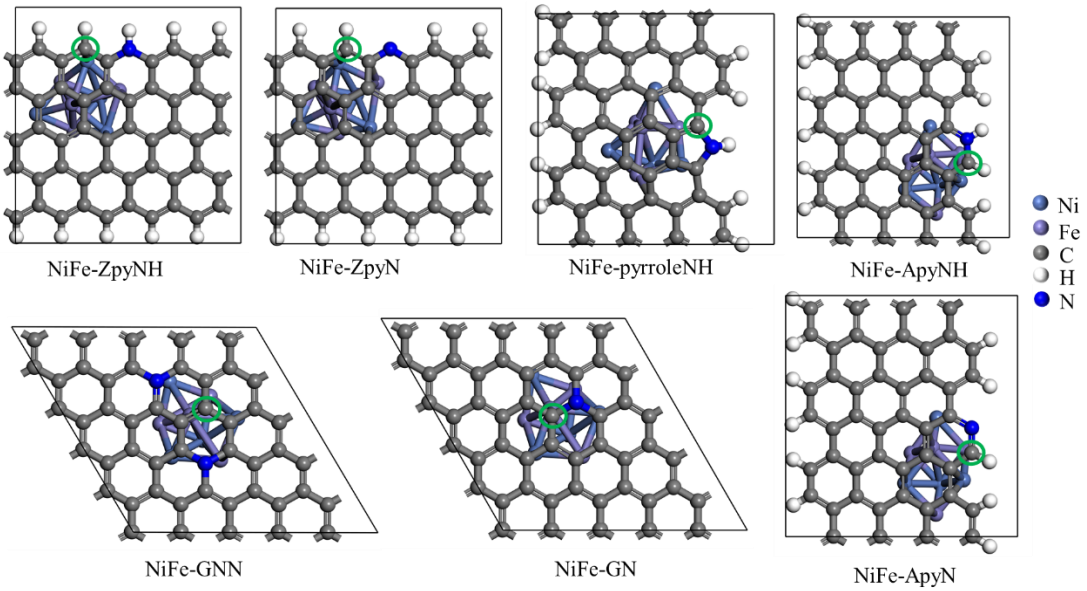

Figure S19 graphene-covered NiFe clusters.

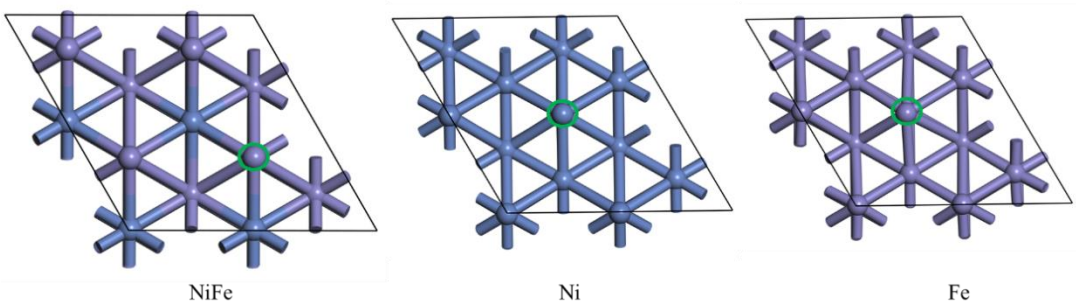

Figure S20 Ni, Fe and NiFe alloy structures.

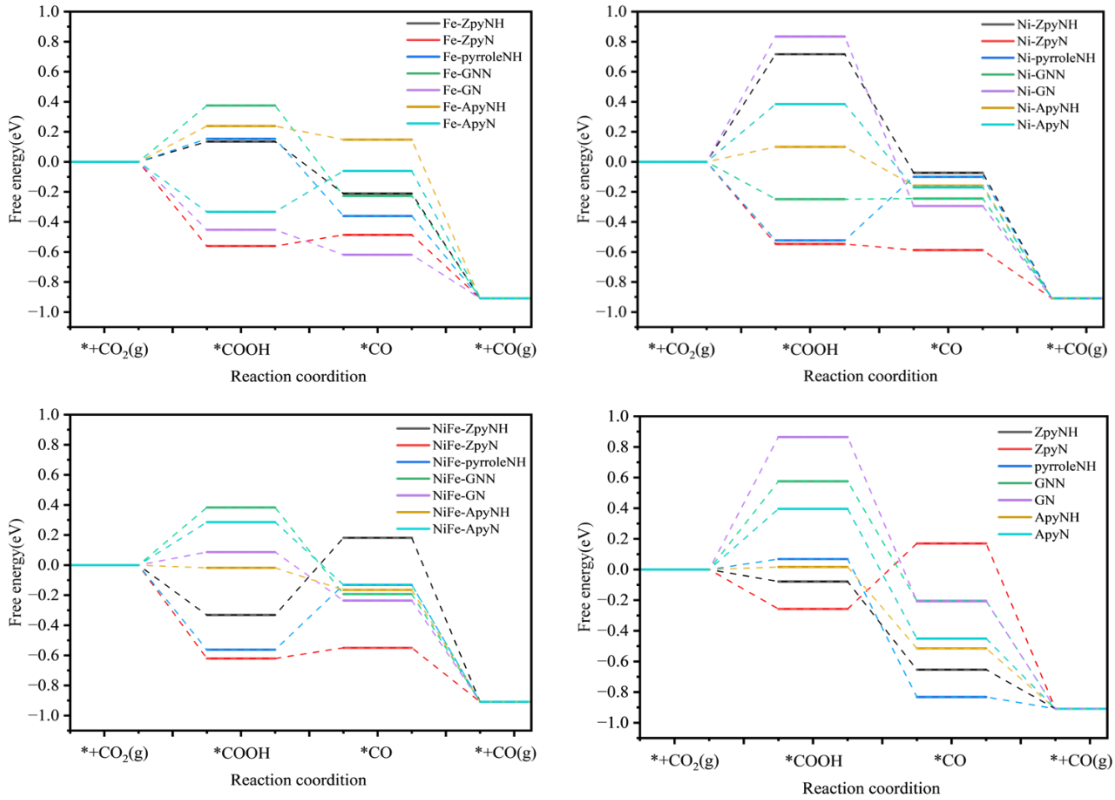

Figure S21 The free energy diagrams (FED) of CO_2RR.

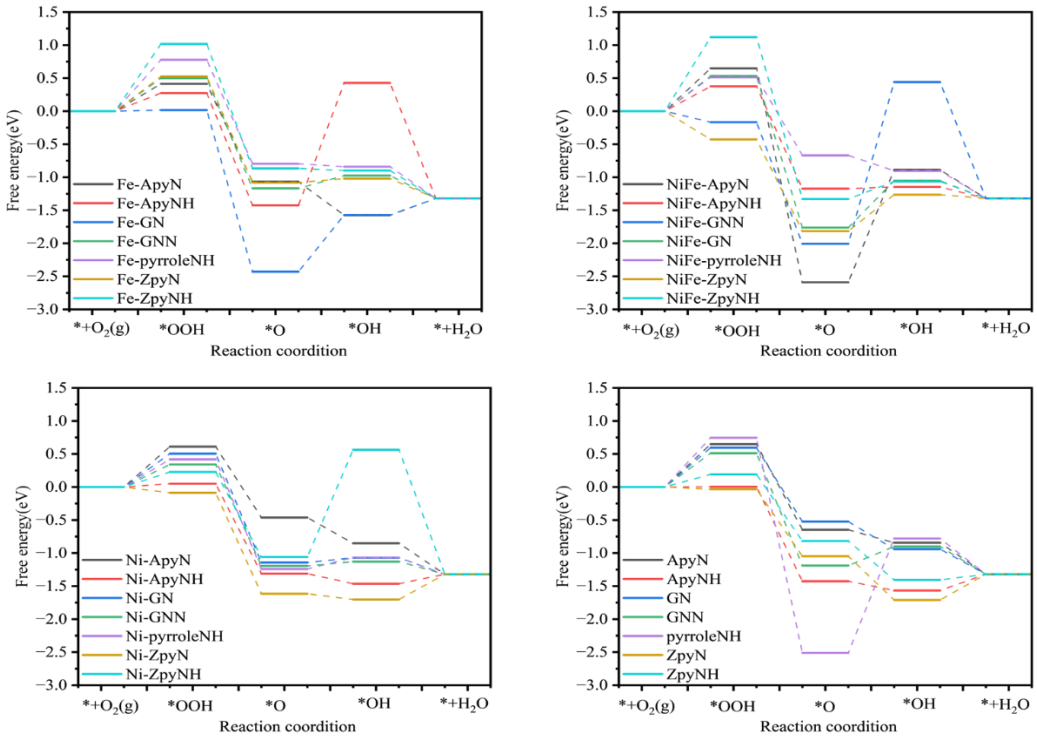

Figure S22 The free energy diagrams (FED) of ORR.

Table S1 The correction from the zero-point energy, entropy and heat capacity for converting the total energies to Gibbs free energies (units: eV). All the associated values are taken from these references[10-14].

Species	ZPE	TS	$\int C_p dT$
COOH*	0.41	0.17	0.09
CO*	0.11	0.08	0.05
*OOH	0.37	0	0
*O	0.072	0.038	0.025
*OH	0.4	0	0
H_2	0.27	0.42	0.09
H_2O	0.58	0.42	0.09

Table S2 Summary of electrochemical CO_2 reduction to CO in a flow cell for different catalysts reported in the literature compared to our work.

Catalyst	**Loading (mg cm^{-2})**	**Catholyte**	**Cathode potentials**	**J_{CO} (mA cm^{-2})**	**CO FE (%)**	**Reference**
NiFe-NC	1.0	3 M KCl	-1.19 V vs. RHE	241.09	91.6	This work
NiFe-NC	1.0	3 M KCl	-0.59 V vs. RHE	63.14	98.88	This work
Ni-NCN	2.0	0.5 M $KHCO_3$	-1.13 V vs. RHE	102.4	97.9	[15]
Cu-In/PNGC	1.0	0.5 M $KHCO_3$	-0.7 V vs. RHE	136.4	91.3	[16]
Ni-N-C	2.0	1 M KOH	-1.18 V vs. RHE	~726	~91	[17]
NiSAs/FN-CNSs)	0.5	2 M $KHCO_3$	2.5 V	175	＞90	[18]
CA/N-Ni	1.0	1 M $KHCO_3$	-0.9 V vs. RHE	300	91	[19]

References:

1. P. Giannozzi, S. Baroni, N. Bonini, M. Calandra, R. Car, C. Cavazzoni, D. Ceresoli, G. L. Chiarotti, M. Cococcioni, I. Dabo, A. Dal Corso, S. de Gironcoli, S. Fabris, G. Fratesi, R. Gebauer, U. Gerstmann, C. Gougoussis, A. Kokalj, M. Lazzeri, L. Martin-Samos, N. Marzari, F. Mauri, R. Mazzarello, S. Paolini, A. Pasquarello, L. Paulatto, C. Sbraccia, S. Scandolo, G. Sclauzero, A. P. Seitsonen, A. Smogunov, P. Umari and R. M. Wentzcovitch, QUANTUM ESPRESSO: a modular and open-source software project for quantum simulations of materials, *J Phys-Condens Mat*, 2009, **21**, 395502.
2. J. K. Norskov, J. Rossmeisl, A. Logadottir, L. Lindqvist, J. R. Kitchin, T. Bligaard and H. Jonsson, Origin of the overpotential for oxygen reduction at a fuel-cell cathode, *J Phys Chem B*, 2004, **108**, 17886-17892.
3. S. Kozuch and J. M. Martin, The rate-determining step is dead. Long live the rate-determining state!, *Chemphyschem*, 2011, **12**, 1413-1418.
4. K. S. Exner and H. Over, Kinetics of Electrocatalytic Reactions from First-Principles: A Critical Comparison with the Ab Initio Thermodynamics Approach, *Acc Chem Res*, 2017, **50**, 1240-1247.
5. J. Chen, Y. Chen, P. Li, Z. Wen and S. Chen, Energetic Span as a Rate-Determining Term for Electrocatalytic Volcanos, *ACS Catalysis*, 2018, **8**, 10590-10598.
6. S. S. S. Kozuch, How to Conceptualize Catalytic Cycles? The Energetic Span Model, *Acc. Chem. Res.*, 2011, 101-110.
7. K. Li, M. Ji, R. Chen, Q. Jiang, J. Xia and H. Li, Construction of nitrogen and phosphorus co-doped graphene quantum dots/Bi_5O_7I composites for accelerated charge separation and enhanced photocatalytic degradation performance, *Chinese Journal of Catalysis*, 2020, **41**, 1230-1239.
8. J. K. R. Nørskov, J.; Logadottir, A.; Lindqvist, L; Kitchin, J.R.; Bligaard, T.; Jonsson,H.;, Origin of the Overpotential for Oxygen Reduction at a Fuel-Cell Cathode, *J. Phys. Chem. B*, 2004, **2004**, 17886-17892.
9. G. Chai, C. Lin, J. Wang, M. Zhang, J. Wei and W. Cheng, Density Functional Theory Simulations of Structures and Properties for Ag-Doped ZnO Nanotubes, *The Journal of Physical Chemistry C*, 2011, **115**, 2907-2913.
10. L. C. Grabow and M. Mavrikakis, Mechanism of Methanol Synthesis on Cu through CO_2 and CO Hydrogenation, *ACS Catalysis*, 2011, **1**, 365-384.
11. H. A. Hansen, J. B. Varley, A. A. Peterson and J. K. Norskov, Understanding Trends in the Electrocatalytic Activity of Metals and Enzymes for CO_2 Reduction to CO, *J Phys Chem Lett*, 2013, **4**, 388-392.
12. P. Hirunsit, Electroreduction of Carbon Dioxide to Methane on Copper, Copper–Silver, and Copper–Gold Catalysts: A DFT Study, *The Journal of Physical Chemistry C*, 2013, **117**, 8262-8268.

13. M. Karamad, H. A. Hansen, J. Rossmeisl and J. K. Nørskov, Mechanistic Pathway in the Electrochemical Reduction of CO_2 on RuO_2, *ACS Catalysis*, 2015, **5**, 4075-4081.
14. M. Liu, Y. Pang, B. Zhang, P. De Luna, O. Voznyy, J. Xu, X. Zheng, C. T. Dinh, F. Fan, C. Cao, F. P. de Arquer, T. S. Safaei, A. Mepham, A. Klinkova, E. Kumacheva, T. Filleter, D. Sinton, S. O. Kelley and E. H. Sargent, Enhanced electrocatalytic CO_2 reduction via field-induced reagent concentration, *Nature*, 2016, **537**, 382-386.
15. C. Lv, K. Huang, Y. Fan, J. Xu, C. Lian, H. Jiang, Y. Zhang, C. Ma, W. Qiao, J. Wang and L. Ling, Electrocatalytic reduction of carbon dioxide in confined microspace utilizing single nickel atom decorated nitrogen-doped carbon nanospheres, *Nano Energy*, 2023, **111**, 108384.
16. X. Zhang, Y. Zhu, Z. Liu, F. Li, W. Zhou, Z. Dong, J. Fan, L. Liu and C. Du, Perforated nitrogen-rich graphene-like carbon nanolayers supported Cu-In catalyst for boosting CO_2 electroreduction to CO, *Journal of Energy Chemistry*, 2022, **75**, 383-390.
17. Y. Li, N. M. Adli, W. Shan, M. Wang, M. J. Zachman, S. Hwang, H. Tabassum, S. Karakalos, Z. Feng, G. Wang, Y. C. Li and G. Wu, Atomically Dispersed Single Ni Site Catalysts for High-efficiency CO_2 Electroreduction at Industrial-level Current Densities, *Energy & Environmental Science*, 2022, **15**, 2108-2119.
18. G. Wang, J. Chen, K. Li, J. Huang, Y. Huang, Y. Liu, X. Hu, B. Zhao, L. Yi, T. W. Jones and Z. Wen, Cost-effective and Durable Electrocatalysts for Co-electrolysis of CO_2 Conversion and Glycerol Upgrading, *Nano Energy*, 2022, **92**, 106751.
19. Y. Zhang, X. Wang, S. Zheng, B. Yang, Z. Li, J. Lu, Q. Zhang, N. M. Adli, L. Lei, G. Wu and Y. Hou, Hierarchical Cross-Linked Carbon Aerogels with Transition Metal-Nitrogen Sites for Highly Efficient Industrial-Level CO_2 Electroreduction, *Advanced Functional Materials*, 2021, **31**, 2104377.